

# $b\bar{b}$ Kinematic Correlations in Cold Nuclear Matter

R. Vogt<sup>1,2</sup>

<sup>1</sup>*Nuclear and Chemical Sciences Division, Lawrence Livermore National Laboratory, Livermore, CA 94551, USA*

<sup>2</sup>*Physics Department, University of California, Davis, CA 95616, USA*

**Background:** The LHCb Collaboration has studied a number of kinematic correlations between  $B$ -hadron pairs through their subsequent decays to  $J/\psi$  pairs at 7 and 8 TeV for four minimum values of the  $J/\psi$   $p_T$ . **Purpose:** In this work, these measurements are compared to calculations of  $b\bar{b}$  pairs and their hadronization and inclusive decays to  $J/\psi J/\psi$  are compared to the same observables. Potential cold matter effects on the  $b\bar{b}$  pair observables are discussed to determine which are most likely to provide insights about the system and why. **Methods:** The calculations, employing the exclusive HVQMNR code, assume the same intrinsic  $k_T$ -broadening and fragmentation as in Ref. [1]. The pair distributions presented by LHCb are calculated in this approach, both for the parent  $b\bar{b}$  and the  $J/\psi J/\psi$  pairs produced in their decay. The sensitivity of the results to the intrinsic  $k_T$  broadening is shown. The theoretical uncertainties due to the  $b$  quark mass and scale variations on both the initial  $b\bar{b}$  pairs and the resulting  $J/\psi$  pairs are also shown. Possible effects due to the presence of the nucleus are studied by increasing the size of the  $k_T$  broadening and modification of the fragmentation parameter. **Results:** Good agreement with the LHCb data is found for all observables. The parent  $b\bar{b}$  distributions are more sensitive to the  $k_T$  broadening than are the final-state  $J/\psi$  pairs. **Conclusions:** Next-to-leading order calculations with  $k_T$  broadening, as in Ref. [1], can describe all correlated observables. Multiple measurements of correlated observables are sensitive to different nuclear effects which can help distinguish between them.

## I. INTRODUCTION

Heavy flavor pair production has long been of interest in elementary  $p + p$  and  $p + \bar{p}$  collisions as a way to test perturbative QCD. Measurements of heavy flavor correlations provide information about how heavy quark pairs are produced in perturbative QCD, indeed much more information that can be gained from single inclusive heavy flavor production alone. In the case of  $b\bar{b}$  production, measurements of pair observables can improve measurements of  $B^0 - \bar{B}^0$  mixing [2]. Finally, a good understanding of multiple correlated observables provides a better baseline for their production and modification in heavy-ion collisions.

Correlated  $b\bar{b}$  studies have been carried out at hadron colliders. The first measurements were in  $p + \bar{p}$  collisions and carried out at the CERN  $Spp\bar{p}S$ , UA1 ( $\sqrt{s} = 0.63$  TeV) [2] and Fermilab Tevatron, D0 ( $\sqrt{s} = 1.8$  TeV) [3], and CDF ( $\sqrt{s} = 1.8$  TeV [4] and  $\sqrt{s} = 1.96$  TeV [5]). These measurements were primarily through studies of lepton pairs. The backgrounds for these measurements include  $c\bar{c}$  decays, Drell-Yan dileptons and leptons from light meson decays. The light hadron decay leptons can be removed by like-sign subtraction. The Drell-Yan rate is much lower than heavy flavor production because it is an electroweak process. In addition, if relatively high  $p_T$  leptons are selected, the charm rate will be suppressed. CDF [4] and, more recently, at the LHC, ATLAS [6] studied  $B$  hadron pair production through  $J/\psi$ +lepton final states in  $p + \bar{p}$  collisions at  $\sqrt{s} = 1.8$  TeV and  $p + p$  collisions at  $\sqrt{s} = 8$  TeV respectively.

More recent measurements of heavy flavor contributions to low mass dilepton production in  $p + p$  collisions have been reported by PHENIX at the BNL relativistic heavy-ion collider ( $\sqrt{s} = 0.2$  TeV) [7] and ALICE at

the LHC ( $\sqrt{s} = 7$  TeV [8] and 13 TeV [9]). In these measurements, the low mass kinematic region of interest makes the  $c\bar{c}$  contributions larger so that both contributions have to be taken into account in the analysis.

Previous dilepton analyses [2–4, 6] have generally focused on tests of NLO calculations, usually in conjunction with diagrams of different topologies in a leading order event generator such as ISAJET [10], HVQJET [11], HERWIG [12] or PYTHIA [13]. For example, UA1 compared calculations at next-to-leading order made with the HVQMNR code [14] to ISAJET as long as its “higher” order contributions (flavor excitation and gluon splitting) were included. They tried to separate different topologies but the results were rather inconclusive due to momentum requirements and statistics. They did, however, determine that the NLO contribution was at least 40% of the measured cross section, depending on the muon  $p_T$  [2]. The D0 Collaboration compared their data to calculations with HVQJET. They showed that their measured azimuthal separation,  $|\Delta\phi|$ , between the decay leptons was compatible with HVQJET with higher order corrections and not with the leading order contributions alone [3]. The CDF measurement at  $\sqrt{s} = 1.8$  TeV [4] compared their final-state  $J/\psi$ +lepton data to HVQMNR calculations as well as to PYTHIA and HERWIG simulations. They found that  $\sim 25\%$  of the  $b\bar{b}$  production as a function of azimuthal separation was found at  $|\Delta\phi| < 90^\circ$ , suggesting the importance of higher-order corrections. CDF also studied the dependence of the  $|\Delta\phi|$  distribution to the bottom quark mass, factorization and renormalization scales, and the intrinsic  $k_T$ . They found that mass and scale variations could alter the magnitude of the cross section but not its shape: changing the shape of the distribution was only possible by modifying the  $k_T$  [4]. These findings are in accord with the

hadron-level studies of  $b\bar{b}$  correlations in Ref. [1]. ATLAS compared their final-state  $J/\psi$ +lepton results with several event generators, finding good agreement between the simulations and the data [6]. The low mass dilepton measurements of PHENIX attempted to separate the dilepton data into  $c\bar{c}$  and  $b\bar{b}$  components, as well as separating the heavy flavor cross sections into their topological components, as if they were independent production mechanisms [7].

Most of the measurements mentioned so far have focused on the central rapidity region. The LHCb Collaboration [15] is the first to study  $b\bar{b}$  correlations through  $J/\psi J/\psi$  final states and at forward rapidity. While such a measurement is less direct than reconstructed  $D$  or  $B$  mesons, as discussed in Ref. [1], along with comparison to  $D\bar{D}$  pairs measured by CDF at  $\sqrt{s} = 1.96$  TeV [16] and LHCb at  $\sqrt{s} = 7$  TeV [17] and  $B$  hadron- $b$  jet pairs measured by CMS at  $\sqrt{s} = 7$  TeV [18], it allows a more straightforward comparison to calculations than the dilepton decay channel.

In this work, the model of  $Q\bar{Q}$  production developed in Ref. [1], with modified Peterson function parameters and  $k_T$  broadening, is employed to study  $b\bar{b} \rightarrow J/\psi J/\psi$  pair production. The measurement is discussed in more detail in Sec. II. In Sec. III, the model employed for  $b\bar{b}$  production is briefly discussed. The pair observables are calculated both for the initial  $b\bar{b}$  production and the final  $J/\psi J/\psi$  pairs, assuming the same minimum  $p_T$  for both the parent  $B$  meson and the decay  $J/\psi$  in Sec. IV. The results are compared and contrasted for the LHCb observables as well as their dependence on the chosen experimental  $p_T$  cut. Section V shows how neglecting  $k_T$  broadening affects the calculated observables. The mass and scale dependence of the results and how they change with  $p_T$  cut is discussed in Sec. VI. Section VII describes possible nuclear effects on the correlations. The work is then summarized in Section VIII.

## II. LHCb MEASUREMENT OF $b\bar{b} \rightarrow J/\psi J/\psi X$

LHCb reconstructed two  $J/\psi$ s from their decays to dimuons in the forward rapidity region,  $2 < y < 4.5$ . The two  $J/\psi$ s must be associated with the same primary vertex to ensure that they came from the same collision. The  $J/\psi$ s were also required to be displaced from their primary vertex to be  $b$  decay candidates. This requirement essentially eliminated prompt  $J/\psi$ s from different collisions as well as events with two prompt  $J/\psi$ s and associated  $J/\psi$  and  $b$  quark production.

They chose different minimum  $J/\psi$  transverse momenta,  $p_T$ , to study the effect of an increasing minimum  $p_T$  on the pair correlations. The data from proton-proton collisions at  $\sqrt{s} = 7$  and 8 TeV were combined for greater statistics. Because the shapes of the distributions at this energy are independent of  $\sqrt{s}$  even if the production cross sections differ, the results were presented as  $(1/\sigma)d\sigma/dX$  where  $X$  refers to the pair observable. This way of dis-

playing the data makes it easier to compare the shapes of the distributions with different minimum  $p_T$ .

LHCb presented results for six pair observables,  $|\Delta\phi^*|$ , the difference in azimuthal angle between the  $b$  and  $\bar{b}$  mesons;  $|\Delta\eta^*|$ , the difference in pseudorapidity between the  $b$  and  $\bar{b}$  mesons;  $A_T$ , the asymmetry between the transverse momenta of the  $J/\psi$ s; and the mass,  $M$ , transverse momentum,  $p_{T_p}$ , and rapidity,  $y_p$  of the  $J/\psi$  pair. The first two observables,  $|\Delta\phi^*|$  and  $|\Delta\eta^*|$ , were assumed to be directly related to the parent  $b$  mesons because  $\phi^*$  and  $\eta^*$  were estimated from the direction of the vector from the primary vertex to the  $J/\psi$  decay vertex [15]. They also included, in an appendix, the distributions  $|\Delta\phi|$ ,  $|\Delta\eta|$ , and  $|\Delta y|$ , the differences in azimuthal angle, pseudorapidity, and rapidity respectively between the  $J/\psi$  mesons themselves. In this work,  $|\Delta y|$  is presented rather than  $|\Delta\eta|$  for the parent  $b\bar{b}$ . All the pair observables studied by LHCb will be calculated for both the parent  $b\bar{b}$  mesons and the subsequent  $J/\psi J/\psi$  decays.

In Ref. [15], the LHCb Collaboration compared their data to PYTHIA [19, 20] and POWHEG [21] calculations as well as simulations of uncorrelated  $b\bar{b}$  production [22, 23] based on the transverse momentum and rapidity distributions for single  $b \rightarrow J/\psi X$  decays measured by LHCb. They noted that the pair distributions generated by both PYTHIA6 [19] and PYTHIA8 [20] were identical and thus the results from the two simulations were combined in their comparison to the data.

As in a number of the previous  $b\bar{b}$  measurements analyzed via dilepton decays [2–4], LHCb looked for evidence of different topological contributions to heavy flavor production in their data: gluon splitting, flavor excitation and flavor creation.

As discussed in detail in Ref. [1], these artificial designations are not indicative of different production mechanisms but of distinct diagram topologies at leading order (flavor creation) and next-to-leading order (including gluon splitting and flavor excitation). No new production mechanism is involved because most of the  $b\bar{b}$  pair production at collider energies is through the  $gg$  initial state which includes all of the aforementioned processes. The distinction was artificially introduced in PYTHIA to separate the true LO diagrams with a  $Q\bar{Q}$  pair in the final state from LO diagrams with either one (flavor excitation) or no (gluon splitting) heavy quarks in the final state. (This separation is necessary because PYTHIA includes only LO diagrams.) Moreover, by treating the different contributions to  $gg \rightarrow Q\bar{Q}X$  production as individual components, not all NLO production diagrams are actually included (such as virtual corrections) and the interferences between diagrams are not accounted for. For more discussion, see Ref. [1].

POWHEG, a NLO generator using PYTHIA for hadronization and decay [21], does not separate these topologies in the same way that PYTHIA does, all diagrams, with their interference terms, are included. In Ref. [15], they conclude that, because POWHEG and PYTHIA both describe the data, NLO effects on  $b\bar{b}$  pro-

duction are small. They also note that, aside from the  $|\Delta\phi^*|$  distributions, the data are consistent with uncorrelated  $b\bar{b}$  production. They reach this conclusion by suggesting that gluon splitting is a small contribution to  $b\bar{b}$  production. However, it is not feasible to separate this diagram from all other NLO contributions because it interferes with the amplitudes of other  $gg$  diagrams.

The conclusion the NLO contributions to  $b\bar{b}$  production are small, reached by the LHCb Collaboration in Ref. [15], can be tested by comparing an NLO calculation of both the  $b\bar{b}$  and  $J/\psi J/\psi$  final states. This comparison, in Sec. IV, is at the center of this work.

### III. MODEL DESCRIPTION

The calculations here follow those outlined in Ref. [1]. The HVQMNR code [14], used here, was designed to calculate  $Q\bar{Q}$  pair production at NLO. As discussed in Ref. [1], the bottom quark mass,  $m_b$ , factorization scale,  $\mu_F$ , and renormalization scale  $\mu_R$  and their uncertainties were set by comparison to the  $b\bar{b}$  total cross section data with  $m_b = 4.65 \pm 0.09$  GeV,  $\mu_F/m = 1.40^{+0.77}_{-0.49}$ , and  $\mu_R/m = 1.10^{+0.22}_{-0.20}$ .

Hadronization was accomplished through the use of the Peterson fragmentation function and  $k_T$  broadening. The value of  $\epsilon_P$ , the Peterson function parameter, was set by comparison to the FONLL  $B$  meson  $p_T$  distribution in Ref. [1] while  $\langle k_T^2 \rangle$ , the average broadening, was fixed previously by comparing the measured  $\Upsilon$   $p_T$  distributions to calculations of  $\Upsilon$  production in the color evaporation model. Here, for  $b\bar{b}$  production,

$$\epsilon_p = 0.0004, \quad (1)$$

$$\langle k_T^2 \rangle = 1 + \frac{\Delta}{3} \ln \left( \frac{\sqrt{s}}{20 \text{ GeV}} \right) \text{ GeV}^2, \quad (2)$$

where the parameter  $\Delta$  was introduced to study the sensitivity of the azimuthal correlations to the amount of broadening. The value  $\Delta = 1$  is the default value [1], resulting in  $\langle k_T^2 \rangle \sim 3 \text{ GeV}^2$  for  $\sqrt{s} = 7 \text{ TeV}$ .

Note that it is necessary to use a code such as the exclusive HVQMNR calculation because the  $Q\bar{Q}$  pair quantities are calculable in such an approach while only single inclusive quark distributions are available with the FONLL [24] and generalized mass - variable flavor number approaches [25, 26]. For further details on the determination of  $\epsilon_P$  and the sensitivity of the  $Q\bar{Q}$  results to the magnitude of  $\langle k_T^2 \rangle$ , see Ref. [1].

Although LHCb suggested in Ref. [15] that the similarity of the PYTHIA and POWHEG simulations are indicative of a small NLO contribution, it is important to recall that gluon splitting is an explicit contribution to  $gg \rightarrow Q\bar{Q}X$  at  $\mathcal{O}(\alpha_s^3)$  and thus a real NLO contribution, as is flavor excitation. As previously discussed, it is not feasible separate out individual diagrams since such a procedure no longer allows for interferences between diagrams. The LO contributions, flavor creation,  $gg \rightarrow Q\bar{Q}$

and  $q\bar{q} \rightarrow Q\bar{Q}$ , only produces back-to-back  $Q\bar{Q}$  pairs, a delta function at  $|\Delta\phi^*| = \pi$  without including broadening. The NLO contributions, modeled in PYTHIA by flavor excitation and gluon splitting and summed together with flavor creation contributions at  $\mathcal{O}(\alpha_s^2)$ , without including interference terms, lead to reduction and broadening of the peak in  $|\Delta\phi|$  at  $|\Delta\phi| = \pi$  with a finite tail as  $|\Delta\phi| \rightarrow 0$ . The introduction of  $k_T$  broadening softens and widens the peak but does not produce a significant enhancement at  $|\Delta\phi| \rightarrow 0$  as it does for charm pairs at similar values of  $p_T$  because  $\langle k_T^2 \rangle < m_b^2$  while, for charm,  $\langle k_T^2 \rangle \sim m_c^2$  [1].

Observables related to the rapidity, either the rapidity difference or the pair rapidity, should be independent of the broadening. However, the other pair observables studied by LHCb should be affected by broadening, at least for the parent  $b$  quarks. Thus the calculations here with compare results with and without  $k_T$  broadening on both the initial  $b\bar{b}$  pairs and the final state  $J/\psi J/\psi$  pairs.

### IV. COMPARISON TO THE LHCb DATA

In this section, the pair quantities,  $|\Delta\phi|$ ,  $|\Delta y|$ ,  $y_p$ ,  $A_T$ ,  $p_{T_p}$  and  $M$  are calculated and compared to the LHCb data. The  $b\bar{b}$  pair distribution include both fragmentation and  $k_T$  broadening as described briefly in the previous section. The  $J/\psi J/\psi$  pair distributions are calculated with the  $B \rightarrow J/\psi X$  decay with a 1.094% branching ratio [27].

All results are shown for the minimum  $p_T$  cuts of 2, 3, 5 and 7 GeV on the  $J/\psi$  and the parent  $B$  meson. Note that the  $J/\psi$ s from  $B$  decay would, of course, generally arise from parent  $B$  mesons with  $p_T$  larger than those of the final-state  $J/\psi$ .

The LHCb data are also shown for comparison on each plot. All quantities are divided by the total cross section,  $(1/\sigma)(d\sigma/dX) \equiv d \ln \sigma / dX$  where  $X$  denotes the observables on the  $y$ -axes of the plots, so that the 7 and 8 TeV LHCb measurements can be combined for improved statistics. Note that even though the LHCb data shown here are from the  $\sqrt{s} = 7$  and 8 TeV runs combined, the  $\sim 15\%$  difference in  $\sqrt{s}$  between the two data sets gives only a 1-2% change in  $\langle k_T^2 \rangle$  based on Eq. (2). Given the small change in  $\langle k_T^2 \rangle$  for  $p+p$  collisions and the uniform shapes of  $d \ln \sigma / dX$ , the calculations compared to the data in this section are all done for  $\sqrt{s} = 7 \text{ TeV}$ .

Note that, in the calculations, the  $J/\psi$ s from  $B$  decays have lower statistics than the parent  $B$  mesons, especially as the minimum  $p_T$  increases. Thus red histograms are generally used to represent the  $J/\psi$  pair quantities while blue curves are used for the  $b\bar{b}$  pair distributions. The LHCb results for  $J/\psi$  pairs are rendered as red points while the reported  $b\bar{b}$  quantities are given as black points.

### A. $|\Delta\phi|$ and $|\Delta\phi^*|$

LHCb presented  $|\Delta\phi|$  distributions for both the initial  $B$  meson pair, reported as  $b\bar{b}$  in Fig. 1 and in all the figures in this section, and the  $J/\psi$  pairs. Recall that LHCb estimated the azimuthal angle of each  $B$  meson from the direction of the vector from the primary vertex to the  $J/\psi$  decay vertex. They also determined the azimuthal angles for the  $J/\psi$ s individually. As shown in Fig. 1, the  $|\Delta\phi^*|$  and  $|\Delta\phi|$  distributions for  $b\bar{b}$  and  $J/\psi J/\psi$  respectively are compatible with each other within the uncertainties.

The  $b\bar{b}$   $|\Delta\phi^*|$  distribution has a peak slightly below  $\Delta\phi \sim \pi$  with a flatter distribution as  $\Delta\phi \rightarrow 0$  relative to that of the  $J/\psi$  pair. As the minimum  $p_T$  grows, the peak near back-to-back ( $\Delta\phi^* \sim \pi$ ) grows higher and becomes narrower for the  $b\bar{b}$  pairs. Likewise, the distribution at  $\Delta\phi^* \sim 0$  starts to increase from approximately flat at low  $\Delta\phi^*$  to a slight enhancement that becomes more pronounced with increasing minimum  $p_T$ . This is because that, as the minimum  $p_T$  grows from 2 to 7 GeV, the relation between  $\langle k_T^2 \rangle^{1/2}$  and  $m_T = \sqrt{p_T^2 + m_b^2}$  goes from  $m_T / \langle k_T^2 \rangle^{1/2} \sim 3$  to  $m_T / \langle k_T^2 \rangle^{1/2} \sim 4.9$ . The larger  $m_T$  allows the development of a double-peaked  $\Delta\phi^*$  distribution, more closely connected to diagrams with a high  $p_T$   $b\bar{b}$  pair balanced against a hard parton in the opposite direction, such as ‘gluon splitting’.

This trend in the increase of  $(\pi/\sigma)d\sigma/d|\Delta\phi|$  can especially be seen for the lighter mass  $J/\psi$  decay products. In this case, because  $m_{J/\psi}/m_b \sim 2/3$  and the minimum  $J/\psi$   $p_T$  is generally smaller than that of the parent  $B$  meson and the  $k_T$  kick is applied to the parent meson, not the  $J/\psi$  decay product, the enhancement seen in the  $b\bar{b}$  distributions sets in at lower  $p_T$  for  $J/\psi$  pairs and is correspondingly larger. Here  $m_{T_\psi} = \sqrt{p_T^2 + m_\psi^2}$  so that  $m_{T_\psi} / \langle k_T^2 \rangle^{1/2} \sim 2.1$  to  $m_{T_\psi} / \langle k_T^2 \rangle^{1/2} \sim 4.4$ , assuming  $p_T^{J/\psi} \equiv p_T^B$ . Because the  $k_T$  kick is on the bottom quarks as they hadronize rather than on the  $J/\psi$  itself, the  $p_T$  selected is larger relative to the primary  $B$  hadron so that the enhancement grows faster with minimum  $p_T$  for  $J/\psi$  pairs, as shown in Fig. 1. If a higher minimum  $p_T$  were chosen for  $B$  mesons, to more closely match the average  $p_T$  of the  $B$  meson producing the minimum  $J/\psi$   $p_T$ , the enhancement at  $|\Delta\phi| \rightarrow 0$  would grow larger, closer to matching the peak at  $|\Delta\phi| \sim \pi$ , as shown for  $c\bar{c}$  correlations with  $p_T > 10$  GeV in Ref. [1].

### B. $|\Delta y|$ and $y_p$

The difference in rapidity,  $\Delta y$ , (or, in the case of the LHCb measurement,  $\Delta\eta$ , was determined both for the initial  $b\bar{b}$  pairs and the final-state  $J/\psi$  pairs. The pair rapidity,  $y_p$ , was only determined for the  $J/\psi$  pairs. Given the acceptance of the LHCb spectrometer of  $2 < y < 4.5$ , the limits on  $\Delta y$  is constrained to be in the range  $0 < \Delta y < 2.5$  while the pair rapidity reported by LHCb lies in the range  $2 < y_p < 4.5$ .

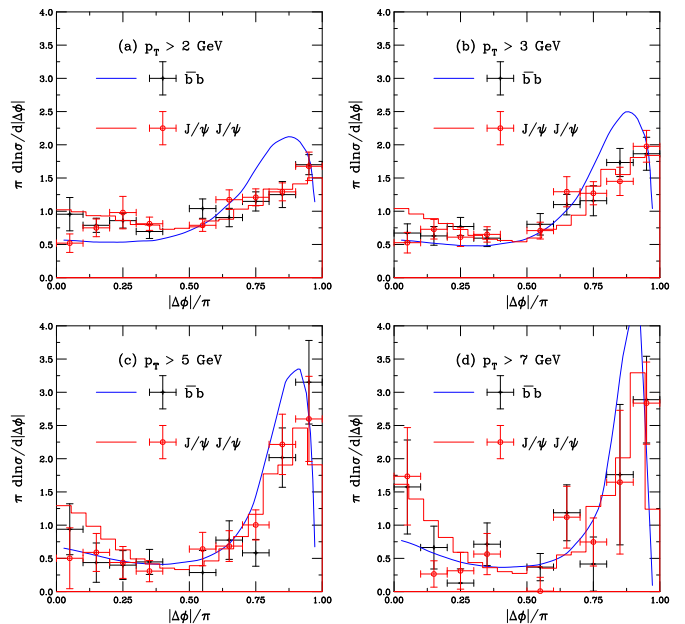


FIG. 1: (Color online) The azimuthal angle difference between the  $b$  and  $\bar{b}$  (blue line) and the  $J/\psi$ 's resulting from the bottom quark decays (red) are shown compared to the LHCb data [15] for the  $p_T$  cuts on the  $b$  quarks and the  $J/\psi$  of 2 (a), 3 (b), 5 (c) and 7 GeV (d).

As is evident from Fig. 2, the  $|\Delta y|$  distribution for  $b\bar{b}$  and  $J/\psi J/\psi$  are in good agreement. The decrease from a peak at  $|\Delta y| = 0$  to 0 at  $|\Delta y| = 2.5$ . The shape of both distributions is more concave than linear but is approximately identical for  $b\bar{b}$  and  $J/\psi J/\psi$ . The behavior is also relatively independent of the minimum  $p_T$ . In the case of the  $b\bar{b}$  pairs, the average  $|\Delta y|$  decreases from 0.75 for  $p_T > 2$  GeV to 0.73 for  $p_T > 7$  GeV, only a 2% difference. On the other hand, the average values of  $|\Delta y|$  for the  $J/\psi$  pairs decreases from 0.74 to 0.69 as the minimum  $p_T$  increases from 2 to 7 GeV. At the highest minimum  $p_T$ , the average  $|\Delta y|$  is reduced by 5% for  $J/\psi$  pairs relative to  $b\bar{b}$  pairs. The differences, while not significant, are not zero.

The pair rapidity distributions, shown in Fig. 3, exhibit a similarly small decrease in the average  $y_p$  with increasing minimum  $p_T$ , a 2% decrease in the average for  $b\bar{b}$  pairs between  $p_T > 2$  and  $> 7$  GeV, from 3.07 to 3.00 respectively. There is a 5% decrease in average  $y_p$  for the  $J/\psi$  pairs, from 3.07 with  $p_T > 2$  GeV to 2.93 with  $p_T > 7$  GeV. This small difference on average is sufficient for a small backward shift between the  $b\bar{b}$  and  $J/\psi J/\psi$  curves for  $p_T > 7$  GeV, especially given the average  $p_T$  for the parent  $B$  mesons of  $J/\psi$ s with the same minimum  $p_T$ .

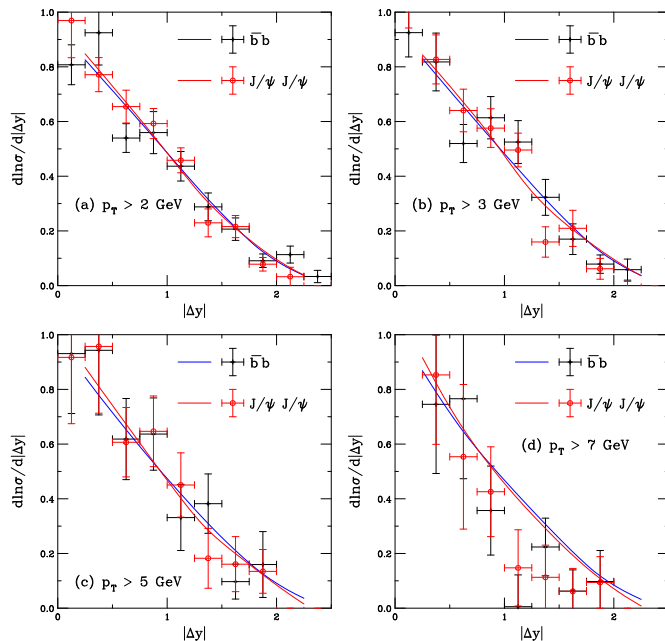


FIG. 2: (Color online) The rapidity difference  $|\Delta y|$  between the  $b$  and  $\bar{b}$  (blue line) and the  $J/\psi$ 's resulting from the bottom quark decays (red) are shown compared to the LHCb data [15] for the  $p_T$  cuts on the  $b$  quarks and the  $J/\psi$  of 2 (a), 3 (b), 5 (c) and 7 GeV (d).

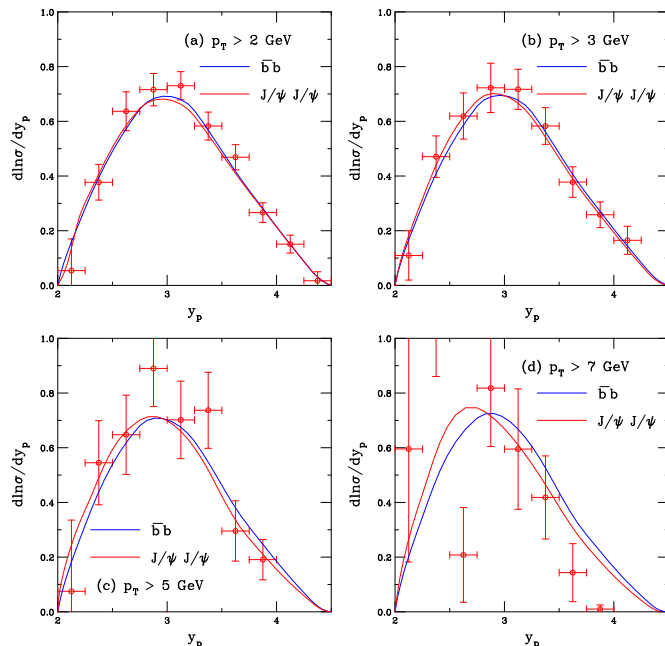


FIG. 3: (Color online) The pair rapidity of the  $b$  and  $\bar{b}$  (blue line) and the  $J/\psi$ 's resulting from the bottom quark decays (red) are shown compared to the LHCb data [15] for the  $p_T$  cuts on the  $b$  quarks and the  $J/\psi$  of 2 (a), 3 (b), 5 (c) and 7 GeV (d).

### C. $A_T$

The  $p_T$  asymmetry,  $A_T = |(p_{T1} - p_{T2})/(p_{T1} + p_{T2})|$ , shown in Fig. 4, would be zero for  $b\bar{b}$  pairs produced in a back-to-back configuration at leading order. At NLO, the pairs are no longer back-to-back and  $d\ln\sigma/dA_T$  decreases with increasing  $A_T$ . The  $A_T$  distribution for the  $J/\psi$  pairs is maximal at  $A_T = 0$ , in accord with the maximum  $|\Delta\phi| \sim \pi$ . This same relation also results in a steeper  $A_T$  distribution for higher minimum  $p_T$ . The distribution goes to zero at  $A_T = 1$  if the  $p_T$  of one of the  $b$  quarks or  $J/\psi$  mesons is very soft or the final states are in alignment.

On the other hand, the  $b\bar{b}$  distributions peak away from  $A_T = 0$  due to the inclusion of  $k_T$  broadening. The peak of the  $A_T$  distribution is at  $A_T \sim 0.25$  for  $p_T > 2$  GeV. As the minimum  $p_T$  is increased, the distribution for  $b\bar{b}$  pairs becomes narrower with a higher peak, akin to the  $|\Delta\phi^*|$  distributions shown in Fig. 1. The average value of  $A_T$  decreases from 0.025 at  $p_T > 2$  GeV to 0.17 at  $p_T > 7$  GeV.

As previously mentioned, the  $J/\psi$  pair  $A_T$  distribution is maximum at  $A_T = 0$  instead of a finite  $A_T$ , as for  $b\bar{b}$ . For lower minimum  $p_T$ , the distribution is narrower for the  $J/\psi J/\psi$ , with an average of  $A_T \sim 0.21$  for  $p_T > 2$  GeV. By the highest minimum  $p_T$ ,  $p_T > 7$  GeV, the average is approximately the same for both,  $A_T \sim 0.16$  for  $J/\psi J/\psi$ .

The trends for the calculated  $J/\psi$  pairs are in very good agreement with the data for all values of minimum  $p_T$  studied. Note also that, above  $A_T \sim 0.4$ , the calculated  $b\bar{b}$  and  $J/\psi J/\psi$  distributions are in agreement.

### D. $p_{T_p}$ and $M$

The last two pair observables measured by LHCb were the pair transverse momentum,  $p_{T_p}$ , and pair mass,  $M$ , distributions, shown in Figs. 5 and 6 respectively.

The  $p_T$  of the pair, shown on a linear scale in Fig. 5, peaks at low  $p_{T_p}$  for both the  $b\bar{b}$  and  $J/\psi J/\psi$  pairs. For the lowest minimum single meson  $p_T$ , while the peaks of the two calculated distributions are of similar magnitude, the  $J/\psi$  pair peak is shifted backward by about 1.7 GeV relative to the  $b\bar{b}$ , as is evident in Fig. 5(a). At  $p_T > 3$  GeV, while the average  $p_{T_p}$  is still about 1.3 GeV smaller for the  $J/\psi$  pairs, most of the difference is at  $p_{T_p} < 5$  GeV. Above this value, the distribution is significantly broader than for  $p_T > 3$  GeV.

As the minimum  $p_T$  is increased, the average values of  $p_{T_p}$  for the initial  $b\bar{b}$  and the final  $J/\psi J/\psi$  become more similar. In addition, a feature develops at high  $p_{T_p}$ , a shoulder in the distribution that appears at effectively twice the minimum  $p_T$ , independent of whether the calculation is for the initial  $b\bar{b}$  pairs or the decay  $J/\psi$  pairs although the statistics at high pair  $p_T$  is significantly degraded for  $p_T > 7$  GeV. The rise of this shoulder appears to correspond to the rise of the peak at  $|\Delta\phi| = 0$  in

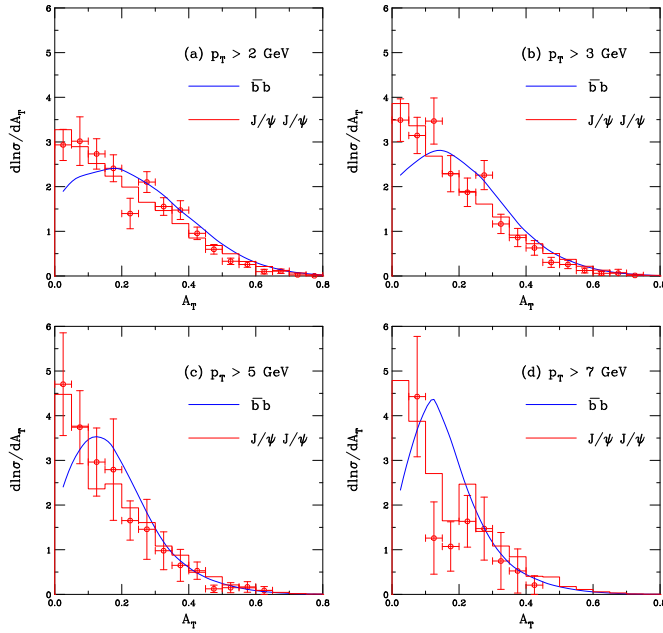


FIG. 4: (Color online) The  $p_T$  asymmetry between the  $b$  and  $\bar{b}$  (blue line) and the  $J/\psi$ 's resulting from the bottom quark decays (red) are shown compared to the LHCb data [15] for the  $p_T$  cuts on the  $b$  quarks and the  $J/\psi$  of 2 (a), 3 (b), 5 (c) and 7 GeV (d).

Fig. 1 where the  $b\bar{b}$  and  $J/\psi$  pairs are aligned. In all cases, however, the calculated  $J/\psi J/\psi$  pair distributions agree quite well with the LHCb data.

A similar trend seen for the pair mass distributions in Fig. 6. The minimum  $b\bar{b}$  pair mass is  $2m_b = 9.3$  GeV for  $m_b = 4.65$  GeV. Assuming that the  $p_T$  of both of the individual mesons are equal, the square of the pair mass can be written as  $M^2 = 2m_T^2(1 + \cosh(\Delta y))$ . Thus as the minimum single meson  $p_T$  increases,  $m_T$  also increases and the average pair mass moves to higher  $M$ . This estimate is accurate for  $2 \rightarrow 2$  processes but is an underestimate for the  $2 \rightarrow 3$  diagrams that dominate NLO  $b\bar{b}$  production. Nonetheless, one can see a clear trend that the  $b\bar{b}$  peak shifts to higher mass with an increase in minimum  $p_T$ , with a residual enhancement at  $2m_b$  for the highest minimum  $p_T$ .

When  $J/\psi$  pairs from  $b$  decays are considered, the pair mass does not have a specific threshold any longer. As shown for  $M > 2m_b$ , the  $J/\psi$  pair mass is steeply decreasing for  $p_T > 2$  and 3 GeV while for  $p_T > 5$  and 7 GeV, a peak at higher  $M$  also develops. The average mass of the  $J/\psi$  pairs for the higher minimum  $p_T$  is shifted backward by several GeV: compare the blue curves and the red histograms in Fig. 6(c) and (d). The calculations of the  $J/\psi$  pairs follow the LHCb data very closely.

In general, the calculations presented here are in very good agreement for the pair observables obtained by LHCb for all values of the minimum  $p_T$  chosen.

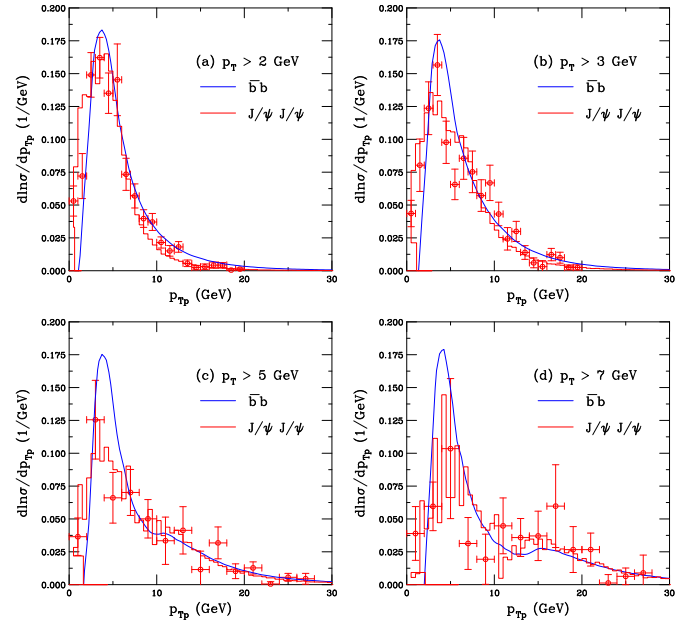


FIG. 5: (Color online) The transverse momentum of the  $b$  and  $\bar{b}$  (blue line) and the  $J/\psi$ 's resulting from the bottom quark decays (red) are shown compared to the LHCb data [15] for the  $p_T$  cuts on the  $b$  quarks and the  $J/\psi$  of 2 (a), 3 (b), 5 (c) and 7 GeV (d).

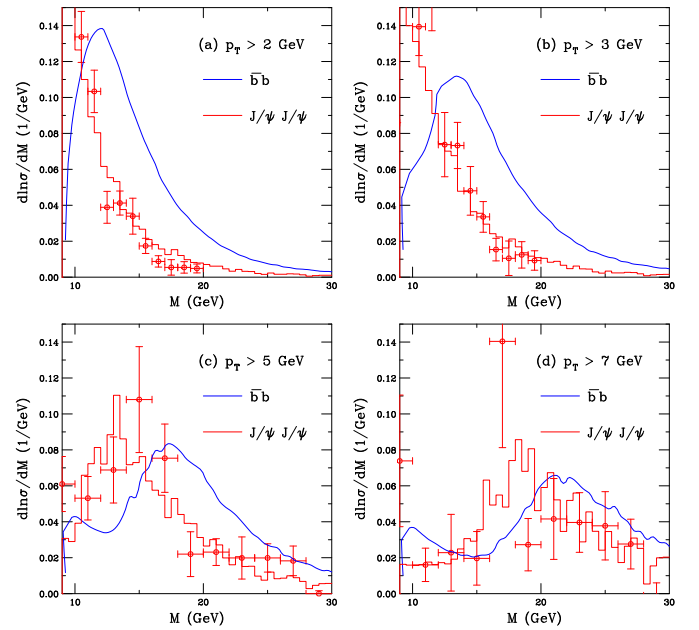


FIG. 6: (Color online) The pair mass of the  $b$  and  $\bar{b}$  (blue line) and the  $J/\psi$ 's resulting from the bottom quark decays (red) are shown compared to the LHCb data [15] for the  $p_T$  cuts on the  $b$  quarks and the  $J/\psi$  of 2 (a), 3 (b), 5 (c) and 7 GeV (d).

## V. SENSITIVITY OF $d\sigma/d\phi$ TO $\langle k_T^2 \rangle$

In this section, the sensitivity of observables to the presence of an intrinsic  $\langle k_T^2 \rangle$  is explored. While in Ref. [1], the sensitivity was studied by gradually dialing up  $\langle k_T^2 \rangle$  to its default value, here only the results with  $\langle k_T^2 \rangle = 0$  and the default 3 GeV<sup>2</sup> (at  $\sqrt{s} = 7$  TeV are compared. The comparison is made for both the  $b\bar{b}$  pairs and the final  $J/\psi J/\psi$ .

Because  $|\Delta y|$  and  $y_p$  are independent of  $\langle k_T^2 \rangle$ , the comparison is only shown for  $|\Delta\phi|$ ,  $M$ ,  $p_{T_p}$  and  $A_T$  in Fig. 7. The left-hand side of the figure shows the results for  $p_T > 2$  GeV while calculations for  $p_T > 7$  GeV are shown on the right-hand side. The behavior of calculations with  $p_T > 3$  and 5 GeV follow similar trends. All results with  $\langle k_T^2 \rangle = 0$  are given in black, curves for  $b\bar{b}$  and histograms for  $J/\psi J/\psi$ .

It is clear that the  $b\bar{b}$  distributions are most affected by the presence of broadening. The peaks at  $|\Delta\phi^*| \sim \pi$ , low  $p_{T_p}$  and low  $A_T$  are enhanced. They are not delta functions without broadening but have finite tails indicative of a NLO process. There is no significant change in the pair mass distributions, independent of minimum  $p_T$ .

On the other hand, the  $J/\psi$  pair distributions are largely unaffected by  $k_T$  broadening even though the parent  $b$  meson pairs show significant dependence on the presence of  $k_T$  broadening. This is because the decay randomizes the direction of the  $J/\psi$  relative to the  $b$  meson parent. Thus it is not possible to learn much about broadening in the initial state by studying the final-state decay products. It would be better to look at the  $B$  meson pair correlations themselves than studying pair observables through the  $J/\psi$  decay products.

## VI. THEORETICAL UNCERTAINTIES

Finally, the mass and scale uncertainties on the  $b\bar{b}$  and their translation to the  $J/\psi$  pair decay products are discussed here. The results for all pair observables are shown for the lowest and highest minimum  $p_T$  values,  $p_T > 2$  GeV in Fig. 8 and  $p_T > 7$  GeV in Fig. 9.

The mass and scale uncertainties are calculated based on results using the one standard deviation uncertainties on the quark mass and scale parameters. If the central, upper and lower limits of  $\mu_{R,F}/m$  are denoted as  $C$ ,  $H$ , and  $L$  respectively, then the seven sets used to determine the scale uncertainty are  $\{(\mu_{F,m}/m, \mu_{F,m}/m)\} = \{(C, C), (H, H), (L, L), (C, L), (L, C), (C, H), (H, C)\}$ . The uncertainty band can be obtained for the best fit sets [28, 29] by adding the uncertainties from the mass and scale variations in quadrature. The envelope contained by the resulting curves,

$$\frac{d\sigma_{\max}}{dX} = \frac{d\sigma_{\text{cent}}}{dX} + \sqrt{\left(\frac{d\sigma_{\mu, \max}}{dX} - \frac{d\sigma_{\text{cent}}}{dX}\right)^2 + \left(\frac{d\sigma_{m, \max}}{dX} - \frac{d\sigma_{\text{cent}}}{dX}\right)^2}, \quad (3)$$

$$\frac{d\sigma_{\min}}{dX} = \frac{d\sigma_{\text{cent}}}{dX} - \sqrt{\left(\frac{d\sigma_{\mu, \min}}{dX} - \frac{d\sigma_{\text{cent}}}{dX}\right)^2 + \left(\frac{d\sigma_{m, \min}}{dX} - \frac{d\sigma_{\text{cent}}}{dX}\right)^2}, \quad (4)$$

defines the uncertainty on the cross section. Here  $X$  is the individual pair observable for a given minimum  $p_T$ . In the calculation labeled “cent”, the central values of  $m$ ,  $\mu_F$  and  $\mu_R$  are used while in the calculations with subscript  $\mu$ , the mass is fixed to the central value while the scales are varied and in the calculations with subscript  $m$ , the mass is varied while the scales are held fixed. The central values of the bottom quark mass,  $\mu_F/m$  and  $\mu_R/m$ , as well as their uncertainties, can be found in Sec. III.

The mass and scale variations do not significantly change the shapes of the distributions relative to the shape of the central value. In addition, changing the minimum  $p_T$  of the integral does not lead to an increase in the widths of the bands. The size of the theoretical uncertainty does not change significantly for the decays to  $J/\psi$  pairs relative to the parent  $b$  and  $\bar{b}$  mesons.

## VII. COLD NUCLEAR MATTER EFFECTS

In Ref. [1], the effects of shadowing and enhanced  $k_T$  broadening on  $c\bar{c}$  production in cold nuclear matter, with the focus on 5.02 TeV  $p$ +Pb collisions, was studied. As discussed there, it has been suggested [31–34] that energy loss by heavy quarks in heavy-ion collisions could change the azimuthal correlations.

However, it must first be ascertained how the heavy flavor pair distributions are influenced by the presence of cold nuclear matter. For example, additional  $k_T$  broadening may be present with a nuclear target due to multiple scattering with nucleons along the path of the initial proton (or nucleus). The strength of the effect depends on the impact parameter of the collision. Energy loss in matter, on the other hand, may result in a shift of the transverse momentum of the heavy quark, akin to a change in the fragmentation function. These effects would be in addition to the modification of the parton densities in the nucleus, referred to as shadowing or nPDF effects, calculated assuming collinear factorization.

Here the focus is on the parent  $b\bar{b}$  correlations instead of their decays to  $J/\psi$  which do not convey as clear of an effect because the decay is isotropic. For illustrative purposes, two particular pair variables are studied out of the six discussed previously: the pair rapidity and the azimuthal separation. Several different scenarios are studied: shadowing alone for both  $p$ +Pb and Pb+Pb collisions; enhanced broadening in  $p$ +Pb collisions; and enhanced broadening with energy loss, represented by an increase in the Peterson function parameter, in Pb+Pb collisions. Shadowing is represented by the central EPS09 NLO shadowing ratio [35] for each of the LHCb  $p_T$  cuts. As noted in Ref. [1] and in Figs. 8 and 9,

if  $\langle k_T^2 \rangle$  is kept fixed, the mass and scale uncertainties do not substantially change the shapes of the distributions.

The central gluon modification of the latest nPDF set, EPPS16 [36], is not significantly different from EPS09. However, EPPS16 has five additional parameters relative to EPS09, resulting in larger uncertainty bands with an uncertainty of 25-30% due to shadowing [37]. Although the uncertainty due to shadowing is significant, it is smaller than the uncertainties due to the heavy quark mass and scale variations, particularly for charm quarks [38]. The larger bottom quark mass and comparably larger scales reduces both the overall uncertainty in the baseline  $p + p$  cross section and the shadowing effect in  $p + p$  and Pb+Pb collisions because of the larger parton momentum fraction accessed and the evolution of the shadowing due to the larger factorization scale. To avoid overlapping ratios in the following figures and better illustrate the effects, only results with the central nPDF set is shown.

In Ref. [1], the sensitivity to the magnitude of  $k_T$  broadening was studied varying the factor  $\Delta$  in Eq. (2) between 0 and 1. So far, in this work,  $\Delta = 1$  has been used as a default. Here, to model broadening in medium,  $\Delta = 2$  is used for  $p + p$  collisions and  $\Delta = 4$  is used in the Pb+Pb calculations. In addition, energy loss in Pb+Pb collisions is modeled by changing the Peterson function parameter,  $\epsilon_P$  from the value used in these calculations heretofore,  $\epsilon_P = 0.0004$  [1] to the default value used previously,  $\epsilon_P = 0.006$  [39]. This change reduces the average  $z$  in the Peterson function from 0.93 to 0.83, a difference of about 10%. See Ref. [1] for the difference in  $\epsilon_P$  makes in the single  $B$  meson  $p_T$  distribution.

The calculations shown here are done at 8.16 TeV for  $p + p$  collisions and 5 TeV for Pb+Pb collisions. The  $p + p$  results used to calculate the nuclear modification factors,  $R_{pPb}$  and  $R_{PbPb}$  respectively, are obtained at the same energies. The same forward rapidity range of the LHCb acceptance is used in these calculations as well. (Note that there is a rapidity shift in  $p + p$  collisions due to the requirement of equal velocity beams at the LHC. However, in the scenario considered here, where the parton momentum fraction,  $x$ , probed by the nucleus, is low, the change in the shadowing ratios is small. If the beam directions were switched, the momentum fraction in the nucleus is in the antishadowing region.)

First, the  $p + p$  distributions calculated at 5 and 8.16 TeV are checked to see if the shapes of the pair distributions are modified at different energies. The slopes remain the same for all  $p_T$  cuts, even at the lowest energy and highest minimum  $p_T$ . Note that this agreement will eventually break down at lower energies, especially for higher  $p_T$ , as one reaches the edge of available phase space, particularly at forward rapidity. Because the shapes of the distributions remain unchanged between 5 and 8.16 TeV, these results are not illustrated.

This section is divided into two subsections, describing the results first for the pair rapidity and then the azimuthal separation between the heavy mesons. In each

part, the nuclear modifications are shown for  $p + p$  and Pb+Pb collisions, both with shadowing alone and then including enhanced  $k_T$  broadening, as well as modification of the fragmentation function in Pb+Pb collisions. While it has already been noted that there is no modification of the  $p + p$  distributions as a function of center of mass energy, some modification of the distributions can be observed in  $p + p$  and Pb+Pb collisions, as will also be shown. Differences can arise with nuclear beams because the momentum fraction probed changes with changing  $\sqrt{s}$ . While  $\sqrt{s}$  changes by only  $\sim 40\%$  between 5 and 8.16 TeV, the shadowing effect can be modified, especially in Pb+Pb collisions where one of the lead nuclei is probed at relatively high momentum fraction,  $x \sim 0.02$ , in the forward rapidity region. In addition, the higher  $p_T$  cut also probes higher  $x$  and larger scales. These effects are present even before any enhanced broadening is included.

### A. Modifications of $y_P$

The modifications on the pair rapidity are shown in Fig. 10. In  $p + p$  collisions at 8.16 TeV, for an average pair rapidity of 3 in the LHCb acceptance,  $x \sim 10^{-4}$  for  $b$  quark production for the minimum  $p_T$  of 2 GeV. The minimum  $x$  remains of this order for all values of the minimum  $p_T$ . Thus one might expect  $R_{pPb} < 1$  for all cases in Fig. 10(a), not just at  $p_T > 2$  GeV. It is not surprising, however, given the  $x$  range, that  $R_{pPb}$  is independent of  $y_P$  since the EPS09 NLO gluon nPDF ratio is flat for  $x < 0.001$ . The factorization scale is also important for the nPDF ratio because the QCD scale evolution reduces the shadowing effect at higher  $p_T$  as well. In addition, the average pair mass, which should be considered when calculating  $x$  instead of the transverse mass of a single  $b$  quark, is  $\sim 15$  GeV for  $p_T > 2$  GeV and  $\sim 23$  GeV for  $p_T > 7$  GeV.

One should also keep in mind that the minimum  $p_T$  represents the minimum of the  $p_T$  integration range and thus includes contributions from all higher  $p_T$ . The average  $p_T$  for a single  $b$  quark is  $\sim 4$  GeV and decreases slowly with  $p_T$  so that larger  $p_T$  values still give a substantial contribution to the integrals. As already mentioned, the average pair mass is a better quantity to use in the estimate of  $x$  in the LHCb kinematics. Especially at higher minimum  $p_T$ , there are still significant contributions to the pair mass even for  $M > 30$  GeV (see Fig. 6(d)) where shadowing is considerably reduced. Thus, as the minimum  $p_T$  is increased in Fig. 10(a), the ratio increases from  $\sim 0.96$  at  $p_T > 2$  GeV to 1.2 for  $p_T > 7$  GeV.

Note also that for  $c\bar{c}$  production, no significant shadowing effects are seen at  $p_T$  greater than a few GeV at similar energies, see Ref. [1]. In fact, if one considered  $J/\psi$  pairs for the same minimum  $p_T$ , it would not be unreasonable to expect  $R_{pPb}$  to be even higher because the  $p_T$  of the parent  $b$  mesons is generally higher, see

Fig. 5.

When the average  $k_T$  broadening is effectively doubled, as in Fig. 10(b), the ratios are still relatively independent of  $y_p$  but the values of  $R_{pPb}$  increase by a few percent relative to calculations with shadowing alone. A large effect is not expected because, even for a doubling of the  $k_T$  kick,  $\langle k_T^2 \rangle = 5 \text{ GeV}^2$  in this case,  $m_T$  is still larger than  $\langle k_T^2 \rangle^{1/2}$  and, as seen in Ref. [1], changing the  $k_T$  kick does not have a large effect on the shape of the single quark  $p_T$  distributions. A much larger effect was seen on the  $c$  and  $b$  quark  $p_T$  distributions by changing the fragmentation function [1].

Figure 10(c) shows the effect of shadowing alone on results from Pb+Pb collisions at 5 TeV. As noted earlier, the  $x$  range probed is slightly higher even though the factorization scale remains the same, due to the lower energy. Now, however, the ratio  $R_{AA}$  is always larger than unity and is no longer independent of  $y_p$  but shows some structure. This is because one of the lead nuclei is now also probing the nPDFs at higher  $x$ ,  $x \geq 0.01$ , and moves through the antishadowing region as  $y_p$  increases. Due to the combination of nuclear effects from both targets,  $R_{AA} > 1$  for all values of the minimum  $p_T$  because, effectively,  $R_{AA}(y_p) = R_{pA}(y_p) \times R_{pA}(-y_p)$  [40].

Perhaps the most intriguing result is seen in Fig. 10(d) where the average  $k_T$  kick is again doubled over that employed in  $p$ +Pb collisions, to  $\langle k_T^2 \rangle \sim 8.4 \text{ GeV}^2$ . (There are, of course, some small variations in  $\langle k_T^2 \rangle$  between 5 and 8.16 TeV due to the energy dependence assumed for  $\langle k_T^2 \rangle$ , given in Eq. (2).) If that was the only effect assumed for Pb+Pb collisions, one would have expected the  $R_{AA}$  to be similar to, but higher than, those in Fig. 10(b). Instead the ratios are now effectively on top of each other at  $y_p \sim 2.5$  with some separation seen at  $y_p \sim 4.5$ . Indeed, the ratio with the highest minimum  $p_T$  is now lowest at the largest  $y_p$ . This is because, in addition to the  $k_T$  broadening, an effective energy loss has been introduced by changing the Peterson fragmentation function parameter from the value determined in Ref. [1], to agree with the FONLL  $b$  meson  $p_T$  distribution, to the  $e^+e^-$  default value,  $\epsilon_P = 0.006$ . As discussed in Ref. [1], this is an effective reduction in the average fraction of momentum transferred from the quark to the meson, from  $\sim 93\%$  with  $\epsilon_P = 0.0004$  to  $\sim 83\%$  for  $\epsilon_P = 0.006$ . Note that this is in no way intended to replace a real energy loss calculation but is rather intended to illustrate the possible effect on  $R_{AA}$  for correlated observables.

The effect of  $k_T$  broadening is to increase the average  $p_T$ , as in Fig. 10(b), while increasing  $\epsilon_P$  decreases it. Because even such a large  $\langle k_T^2 \rangle$  is still smaller than the lowest  $m_T^2$  with a minimum  $p_T$  of 2 GeV, the effect of fragmentation is more important for  $R_{AA}$  as a function of  $y_p$ . The single quark  $p_T$  distribution with  $\epsilon_P = 0.006$  is more steeply falling with  $p_T$  than can be compensated by an increased  $k_T$  broadening. This is even more evident at higher  $p_T$  where the larger  $\epsilon_P$  reduces the fraction of cross section in the  $p_T$  range significantly, see the single  $p_T$  distributions in Ref. [1]. The reduced cross section

due to the change in  $\epsilon_P$  results in the calculated  $R_{AA}$  collapsing on top of each other in Fig. 10(d).

The  $y_p$  distributions are shown for  $p + p$  collisions at  $\sqrt{s} = 7 \text{ TeV}$  (blue);  $p + \text{Pb}$  at  $\sqrt{s_{NN}} = 8.16 \text{ TeV}$  (red); and Pb+Pb collisions at  $\sqrt{s_{NN}} = 5 \text{ TeV}$  (black) for  $p_T > 2$  and 7 GeV in Fig. 11, including all cold matter effects. As one might expect from the discussion in Sec. IV, the  $\Delta y$  and  $y_p$  distributions are unaffected by  $k_T$  broadening. Thus the  $y_p$  distributions for  $p + p$  and  $p + \text{Pb}$  collisions are the same shape. However, the Pb+Pb distribution is clearly shifted backward to lower  $y_p$ , a small but visible effect that increases with minimum  $p_T$ . This is due to the change in  $\epsilon_P$ . The steeper  $p_T$  distributions with the higher value of  $\epsilon_P$  mean that fewer  $b$  quarks may be found at higher rapidity, especially for higher values of the minimum  $p_T$ , reducing the average  $y_p$  in Pb+Pb collisions relative to the other cases.

## B. Modifications of $|\Delta\phi|$

Figure 12, showing  $R_{pPb}$  and  $R_{AA}$  as a function of the azimuthal separation between the  $b$  and  $\bar{b}$ , tells a somewhat different story of enhanced nuclear effects. Note that for shadowing only, both for  $p + \text{Pb}$  and Pb+Pb, a similar pattern as for the  $y_p$  ratios in Fig. 10(a) and (c) is observed. However, the ratios are not entirely independent of  $\Delta\phi$  in this case since some decrease in the ratio is seen as  $\Delta\phi \rightarrow \pi$ . A similar pattern was seen for  $c\bar{c}$  production at 5 TeV in Ref. [1] where the  $R_{pPb}$  shadowing ratios were independent of  $\Delta\phi$  with  $\langle k_T^2 \rangle = 0$  but showed a slight decrease with increasing  $\Delta\phi$  for enhanced broadening. The results shown for  $c\bar{c}$  were, however, integrated over all  $p_T$ . Here, when the minimum  $p_T$  is increased, the change in slope at  $\Delta\phi \rightarrow \pi$  is somewhat sharpened. This can be attributed to the narrowing and sharpening of the peak in the  $\Delta\phi$  distribution with increasing  $p_T$ , seen in Fig. 1, while the enhancement at low  $\Delta\phi$ ,  $\Delta\phi \rightarrow 0$ , is increasing more slowly.

The more striking effect is for  $p + \text{Pb}$  and, in particular, Pb+Pb collisions with enhanced  $k_T$  broadening. As shown in Fig. 13, the effect of broadening on the azimuthal distributions in  $p + \text{Pb}$  and Pb+Pb collisions reduces and broadens the peak at  $\Delta\phi \sim \pi$  and enhances the distribution at  $\Delta\phi \sim 0$ . (The normalized distributions are shown. Recall that these distributions are the same shape in  $p + p$  collisions so that the differences seen in the figure arise only from the CNM effects.) Only the results for the lowest and highest minimum  $p_T$  values are again shown to illustrate the effect.

The  $p + \text{Pb}$  ratios with enhanced  $k_T$  broadening show a kink that occurs at higher  $\Delta\phi$  with increasing minimum  $p_T$ . This can be understood from the ratios of increasing  $\langle k_T^2 \rangle$  relative to the results with no broadening,  $\langle k_T^2 \rangle = 0$  in Ref. [1], showed a turn on of the effect at  $\langle k_T^2 \rangle > 0$ , becoming increasingly isotropic as  $\langle k_T^2 \rangle$  increases. As shown in Ref. [1], the  $\Delta\phi$  distributions peak more sharply at both  $\Delta\phi \rightarrow \pi$  and  $\Delta\phi \rightarrow 0$ . The effect at  $\Delta\phi = 0$  is

reduced in  $b\bar{b}$  production relative to  $c\bar{c}$  since it requires a much harder gluon to balance a more massive  $b\bar{b}$  pair than the lighter  $c\bar{c}$  pair. This change in relative height of the peak for fixed  $\langle k_T^2 \rangle$  and increasing minimum  $p_T$  causes the location of the kink in the ratio to increase from  $\Delta\phi \sim 1.7$  to 2.5 radians as the minimum  $p_T$  increases from 2 to 7 GeV. The increase in  $R_{p\text{Pb}}$  otherwise is of the same origin as that for  $y_p$  shown in Fig. 10.

The hierarchy is again reversed for Pb+Pb collisions, shown in Fig. 12(d). The fragmentation function parameter has almost no effect on the shape of the  $\Delta\phi$  distribution, as also shown in Ref. [1] when integrated over all  $p_T$ . However, it will change the number of  $b\bar{b}$  pairs with both quarks in the rapidity acceptance, as illustrated in Fig. 11, producing the inverted hierarchy of ratios seen here. Note that the larger  $k_T$  kick assumed for Pb+Pb collisions also result in the kink in  $R_{p\text{Pb}}$  seen in Fig. 12(b), moving to lower  $\Delta\phi$ , now between 1.5 to 2.4 radians.

### VIII. SUMMARY

The  $b\bar{b} \rightarrow J/\psi J/\psi$  pair observables measured by LHCb were studied in detail in an exclusive NLO calculation with fragmentation and  $k_T$  broadening developed in Ref. [1]. The calculations reproduced the data very well in all cases and for all  $p_T$  cuts. The sensitivity of the results to the amount of  $k_T$  broadening is shown and, while the direct  $b\bar{b}$  observables are indeed sensitive to the  $k_T$  broadening, the resulting  $J/\psi$  pairs are not since the decays result in a decorrelation. The mass and scale dependence has also been studied and shown not to be

large, as expected for  $b\bar{b}$  production. Finally, we have also shown the nuclear modification factors for enhanced  $k_T$  broadening and fragmentation function modification.

Here we have shown possible cold nuclear matter effects in  $p$ +Pb and Pb+Pb collisions. They are not intended to be definitive but illustrative only. The calculations have demonstrated how effects like broadening and energy loss could be disentangled by specific correlated observables more sensitive to each. Although both observables discussed are affected by the two effects, the pair rapidity is more sensitive to fragmentation which causes the ratios with different minimum  $p_T$  to become similar while the azimuthal correlation depends most strongly on the  $k_T$  broadening, causing the ratios to separate further with minimum  $p_T$ . While we have labeled and modeled the effects as being due to cold nuclear matter, similar decorrelation, as produced by enhanced  $k_T$  broadening, could be due to hot matter effects, as produced in the quark-gluon plasma [31]. A thermal medium also results in heavy quark energy loss, as modeled by the modified  $\epsilon_P$ . These calculations thus suggest additional correlated observables are required to better quantify such effects, regardless of the medium.

**Acknowledgments:** I would like to thank A. Mischke, T. Dahms, and M. Winn for discussions. This work was performed under the auspices of the U.S. Department of Energy by Lawrence Livermore National Laboratory under Contract DE-AC52-07NA27344 and supported by the U.S. Department of Energy, Office of Science, Office of Nuclear Physics (Nuclear Theory) under contract number DE-SC-0004014.

- 
- [1] R. Vogt, Heavy Flavor Azimuthal Correlations in Cold Nuclear Matter, *Phys. Rev. C* **98** (2018) 034907.
  - [2] C. Albajar *et al.* (UA1 Collaboration), Measurement of  $b\bar{b}$  correlations at the CERN  $p\bar{p}$  collider, *Z. Phys. C* **61** (1994) 41.
  - [3] B. Abbot *et al.* (D0 Collaboration), The  $b\bar{b}$  production cross section and angular correlations in  $p\bar{p}$  collisions at  $\sqrt{s} = 1.8$  TeV, *Phys. Lett. B* **487** (2000) 264.
  - [4] D. Acosta *et al.* (CDF Collaboration), Measurements of  $b\bar{b}$  azimuthal production correlations in  $p\bar{p}$  collisions at  $\sqrt{s} = 1.8$  TeV, *Phys. Rev. D* **71** (2005) 092001.
  - [5] T. Aaltonen *et al.* (CDF Collaboration), Measurement of correlated  $b\bar{b}$  production in  $p\bar{p}$  collisions at  $\sqrt{s} = 1960$  TeV, *Phys. Rev. D* **77** (2008) 072004.
  - [6] M. Aaboud *et al.* (ATLAS Collaboration), Measurement of  $b$ -hadron pair production with the ATLAS detector in proton-proton collisions at  $\sqrt{s} = 8$  TeV, *JHEP* **1711** (2017) 062.
  - [7] C. Aidala *et al.* (PHENIX Collaboration), Correlations of  $\mu\mu$ ,  $e\mu$ , and  $ee$  pairs in  $p + p$  collisions at  $\sqrt{s} = 200$  GeV and implications for  $c\bar{c}$  and  $b\bar{b}$  production mechanisms, arXiv:1805.04075.
  - [8] S. Acharya *et al.* [ALICE Collaboration], Dielectron production in proton-proton collisions at  $\sqrt{s} = 7$  TeV, *JHEP* **1809**, 064 (2018).
  - [9] S. Acharya *et al.* [ALICE Collaboration], Dielectron and heavy-quark production in inelastic and high-multiplicity proton-proton collisions at  $\sqrt{s_{NN}} = 13$  TeV, *Phys. Lett. B* **788**, 505 (2019).
  - [10] F. E. Paige and S. D. Protopopescu, Isajet 5.20: A Monte Carlo Event Generator for  $pp$  and  $p\bar{p}$  Interactions, *Conf. Proc. C* **860115**, 213 (1986).
  - [11] Cited in Ref. [3] as: M. Baarmand and F. Paige. HVQ-JET Monte Carlo Event Generator, private communication.
  - [12] G. Corcella *et al.*, HERWIG 6: An event generator for hadron emission reactions with interfering gluons (including supersymmetric processes), *JHEP* **0101**, 010 (2001).
  - [13] T. Sjostrand *et al.*, High-energy physics event generation with PYTHIA 6.1, *Comput. Phys. Commun.* **135**, 238 (2001); arXiv:hep-ph/0308153.
  - [14] M. L. Mangano, P. Nason, and G. Ridolfi, Heavy quark correlations in hadron collisions at next-to-leading order, *Nucl. Phys. B* **373**, 295 (1992).
  - [15] R. Aaij *et al.* (LHCb Collaboration), Study of  $b\bar{b}$  correlations in high energy proton-proton collisions, *JHEP* **11**

- (2017) 030.
- [16] B. Reisert *et al.* [CDF Collaboration], Charm Production Studies at CDF, Nucl. Phys. Proc. Suppl. **170**, 243 (2007).
- [17] R. Aaij *et al.* [LHCb Collaboration], Observation of double charm production involving open charm in pp collisions at  $\sqrt{s} = 7$  TeV, JHEP **1206**, 141 (2012), [JHEP **1403**, 108 (2014)].
- [18] V. Khachatryan *et al.* [CMS Collaboration], Measurement of  $B\bar{B}$  Angular Correlations based on Secondary Vertex Reconstruction at  $\sqrt{s} = 7$  TeV, JHEP **1105**, 136 (2011).
- [19] T. Sjostrand, S. Mrenna and P. Z. Skands, PYTHIA 6.4 physics and manual, JHEP **05** (2006) 026.
- [20] T. Sjostrand, S. Mrenna and P. Z. Skands, A brief introduction to PYTHIA 8.1, Comp. Phys. Comm. **178** (2008) 852.
- [21] S. Frixione, P. Nason, and G. Ridolfi, A positive-weight next-to-leading-order Monte Carlo for heavy flavour hadroproduction, JHEP **0709**, 126 (2007); arXiv:0707.3081 [hep-ph].
- [22] R. Aaij *et al.* [LHCb Collaboration], Measurement of  $J/\psi$  production in  $pp$  collisions at  $\sqrt{s} = 7$  TeV, Eur. Phys. J. C **71**, 1645 (2011).
- [23] R. Aaij *et al.* [LHCb Collaboration], Production of  $J/\psi$  and  $\Upsilon$  mesons in  $pp$  collisions at  $\sqrt{s} = 8$  TeV, JHEP **1306**, 064 (2013).
- [24] M. Cacciari, M. Greco and P. Nason, The  $p_T$  spectrum in heavy flavor hadroproduction, JHEP **05**, 007 (1998).
- [25] B. A. Kniehl, G. Kramer, I. Schienbein and H. Spiesberger, Inclusive  $D^{*+}$  production in  $p\bar{p}$  collisions with massive charm quarks, Phys. Rev. D **71**, 014018 (2005).
- [26] I. Helenius and H. Paukkunen, Revisiting the D meson hadroproduction in general-mass variable flavour number scheme, JHEP **1805**, 196 (2018).
- [27] M. Tanabashi *et al.* [Particle Data Group], Review of Particle Physics, Phys. Rev. D **98**, 030001 (2018).
- [28] R. E. Nelson, R. Vogt and A. D. Frawley, Narrowing the uncertainty on the total charm cross section and its effect on the  $J/\psi$  cross section, Phys. Rev. C **87**, 014908 (2013).
- [29] R. E. Nelson, R. Vogt and A. D. Frawley, in preparation.
- [30] C. Peterson, D. Schlatter, I. Schmitt, and P. Zerwas, Scaling Violations in Inclusive  $e^+e^-$  Annihilation Spectra, Phys. Rev. D **27** (1983) 105.
- [31] M. Nahrgang, J. Aichelin, P. B. Gossiaux and K. Werner, Azimuthal correlations of heavy quarks in Pb + Pb collisions at  $\sqrt{s} = 2.76$  TeV at the CERN Large Hadron Collider, Phys. Rev. C **90**, 024907 (2014).
- [32] M. Younus, U. Jamil and D. K. Srivastava, Correlations of Heavy Quarks Produced at Large Hadron Collider, J. Phys. G **39**, 025001 (2012).
- [33] M. Younus and D. K. Srivastava, Effect of Energy Loss on Azimuthal Correlations of charm and correlated charm decay in collision of lead nuclei at  $\sqrt{s} = 2.76$  ATeV, J. Phys. G **40**, 065004 (2013).
- [34] M. Younus, S. K. Tripathy, P. K. Sahu and Z. Niak, Azimuthal correlations of  $D$ -mesons in  $p+p$  and  $p+\text{Pb}$  collisions at LHC energies, Eur. Phys. J. A **53**, 112 (2017).
- [35] K. J. Eskola, H. Paukkunen and C. A. Salgado, EPS09: A New Generation of NLO and LO Nuclear Parton Distribution Functions, JHEP **0904**, 065 (2009).
- [36] K. J. Eskola, P. Paakkinen, H. Paukkunen and C. A. Salgado, EPPS16: Nuclear parton distributions with LHC data, Eur. Phys. J. C **77**, 163 (2017).
- [37] J. L. Albacete *et al.*, Predictions for Cold Nuclear Matter Effects in  $p+\text{Pb}$  Collisions at  $\sqrt{s_{NN}} = 8.16$  TeV, Nucl. Phys. A **972**, 18 (2018).
- [38] R. Vogt, Shadowing effects on  $J/\psi$  and  $\Upsilon$  production at energies available at the CERN Large Hadron Collider, Phys. Rev. C **92**, 034909 (2015).
- [39] C. Peterson, D. Schlatter, I. Schmitt, and P. Zerwas, Scaling Violations in Inclusive  $e^+e^-$  Annihilation Spectra, Phys. Rev. D **27** (1983) 105.
- [40] A. Andronic *et al.*, Heavy-flavour and quarkonium production in the LHC era: from protonproton to heavy-ion collisions, Eur. Phys. J. C **76**, 107 (2016).

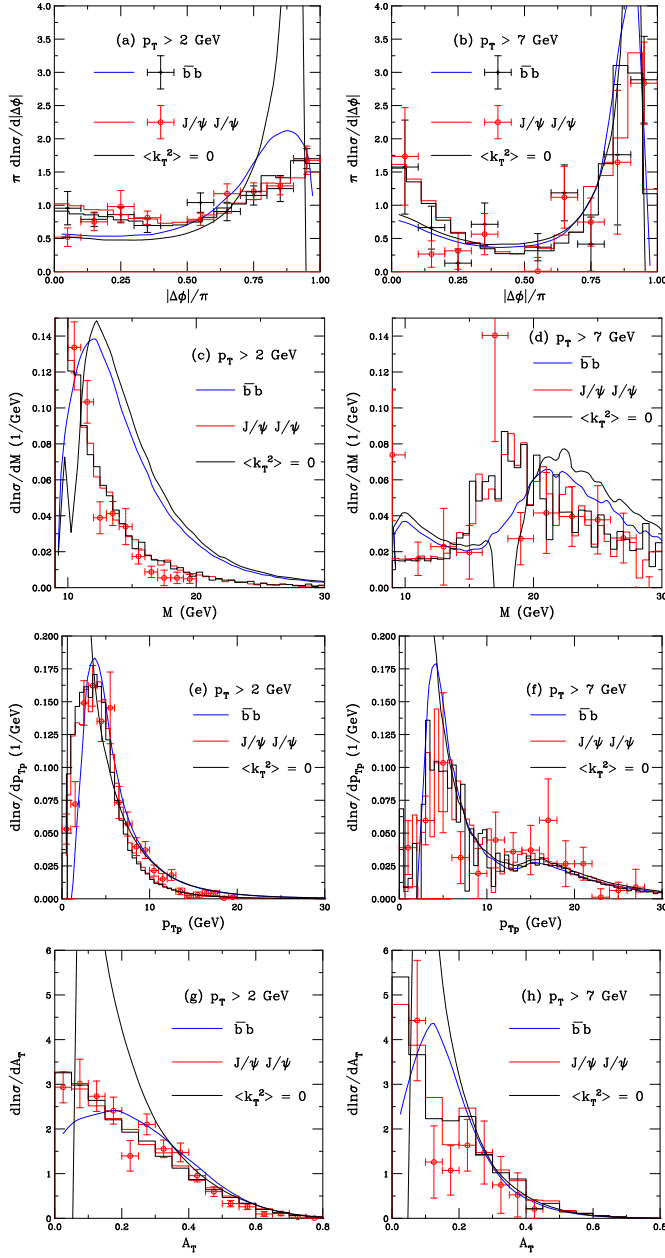


FIG. 7: (Color online) The difference in the  $\bar{b}\bar{b}$  and  $J/\psi J/\psi$  pair results for  $\langle k_T^2 \rangle = 0$  and the default  $k_T$  kick. The  $\langle k_T^2 \rangle = 0$  results are shown by the black curves ( $\bar{b}\bar{b}$ ) and black histograms ( $J/\psi J/\psi$ ) and with the default  $k_T$  kick by the blue curves ( $\bar{b}\bar{b}$ ) and red histograms ( $J/\psi J/\psi$ ). Results are shown for the azimuthal angle difference (a) and (b); pair mass (c) and (d); pair transverse momentum (e) and (f); and  $p_T$  asymmetry (g) and (h). The results on the left-hand side (a), (c), (e) and (g) are shown for  $p_T > 2$  GeV while those on the right-hand side (b), (d), (f) and (h) are shown for  $p_T > 7$  GeV. The LHCb data [15] are also shown.

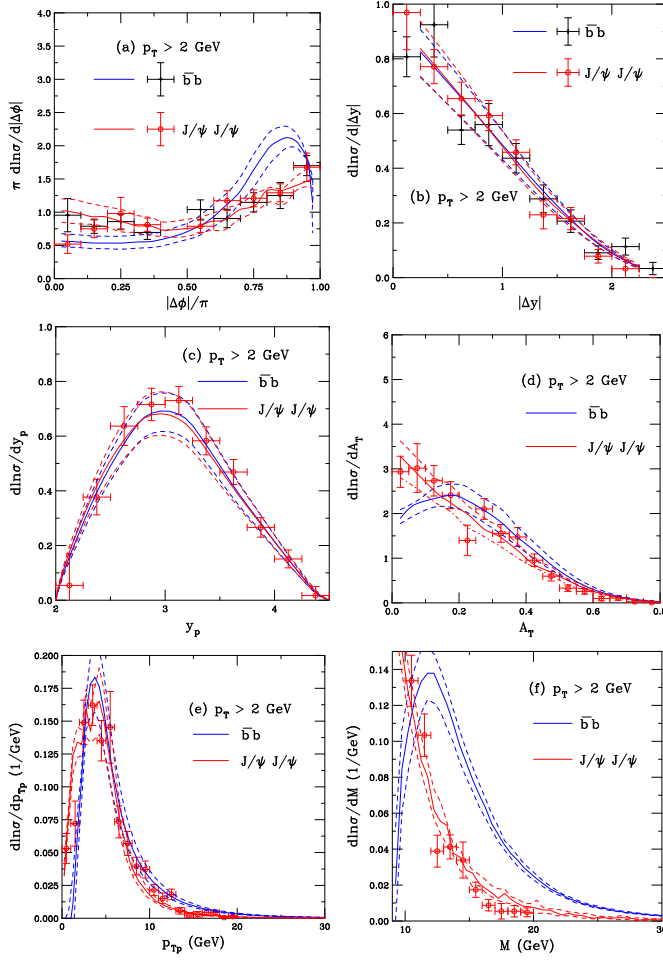


FIG. 8: (Color online) The mass and scale uncertainty bands are shown for the  $b\bar{b}$  pairs (blue curves) and  $J/\psi J/\psi$  pairs (red curves) and compared to the LHCb data [15] for  $p_T > 2$  GeV. The central values are given by the solid curves while the limits on the uncertainties are shown by the dashed curves. Results are given for the azimuthal difference (a); rapidity difference (b); pair rapidity (c);  $p_T$  asymmetry (d); pair  $p_T$  (e); and pair mass (f).

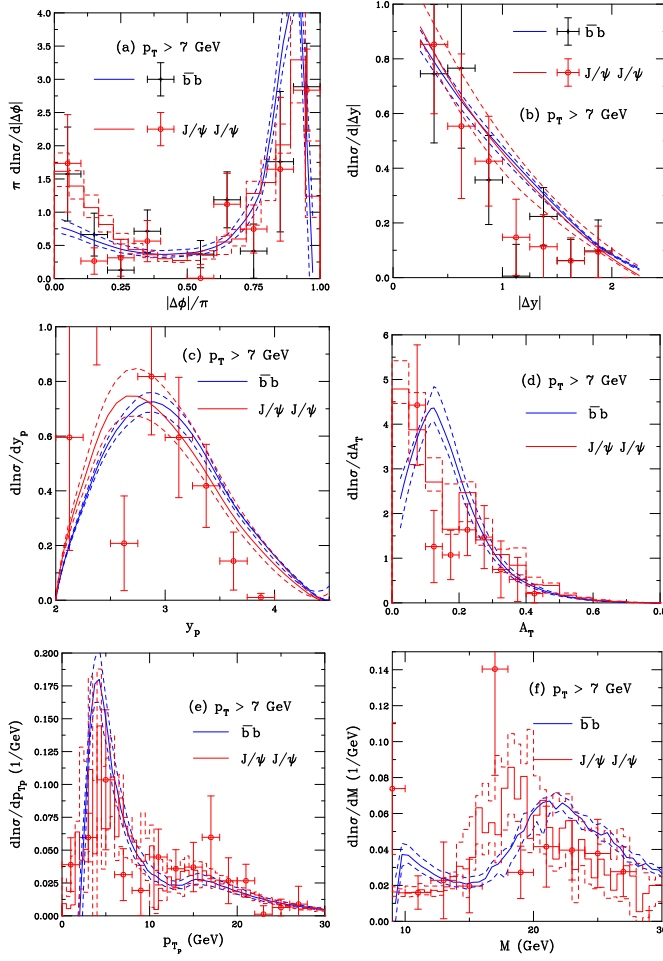


FIG. 9: (Color online) The mass and scale uncertainty bands are shown for the  $b\bar{b}$  pairs (blue curves) and  $J/\psi J/\psi$  pairs (red curves) and compared to the LHCb data [15] for  $p_T > 7$  GeV. The central values are given by the solid curves while the limits on the uncertainties are shown by the dashed curves. Results are given for the azimuthal difference (a); rapidity difference (b); pair rapidity (c);  $p_T$  asymmetry (d); pair  $p_T$  (e); and pair mass (f).

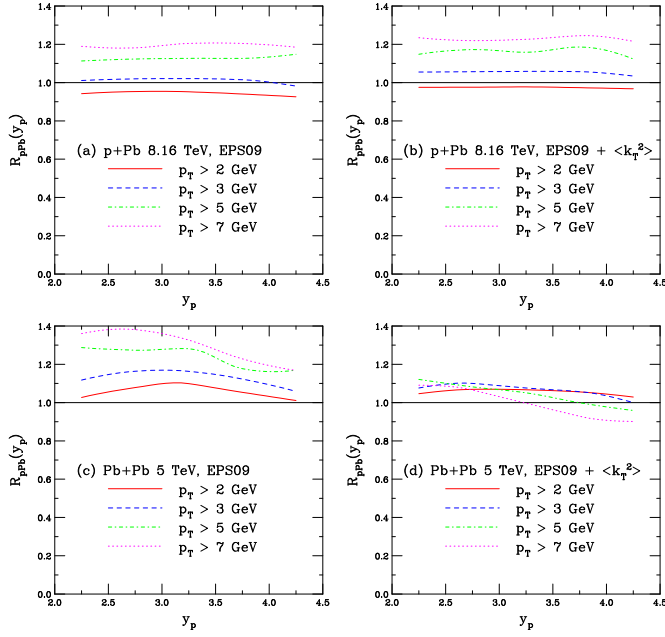


FIG. 10: (Color online) Cold nuclear matter effects on the  $b\bar{b}$  pair rapidity for  $p_T > 2$  (solid red), 3 (dashed blue), 5 (dot-dashed green), and 7 GeV (dotted magenta) for (a)  $p$ +Pb collisions at 8.16 TeV with central EPS09 only (b)  $R_{pPb}$  at 8.16 TeV with EPS09 and additional  $k_T$  broadening, (c) Pb+Pb collisions at 5 TeV with central EPS09 only, and (d)  $R_{AA}$  at 5 TeV with EPS09 and additional  $k_T$  broadening.

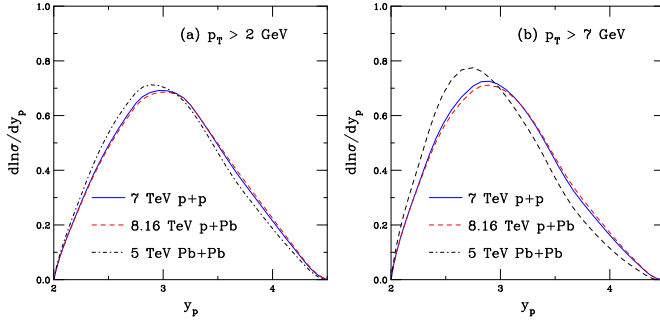


FIG. 11: (Color online) The  $b\bar{b}$  pair rapidity for  $p_T > 2$  (a) and 7 GeV (b) for  $p$ + $p$  collisions at 7 TeV (solid blue),  $p$ +Pb collisions at 8.16 TeV (dashed red) and Pb+Pb collisions at 5 TeV (dot-dashed black). The  $p$ +Pb calculations include shadowing and enhanced broadening ( $2\Delta$ ) while the Pb+Pb calculations include shadowing, broadening ( $4\Delta$ ), and fragmentation function modification.

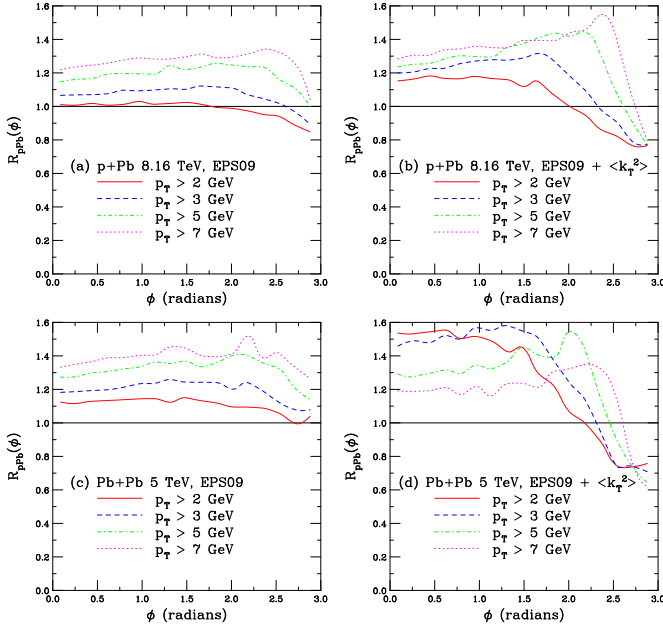


FIG. 12: (Color online) Cold nuclear matter effects on the  $b\bar{b}$  azimuthal angle difference for  $p_T > 2$  (solid red), 3 (dashed blue), 5 (dot-dashed green), and 7 GeV (dotted magenta) for (a)  $p$ +Pb collisions at 8.16 TeV with central EPS09 only (b)  $R_{pPb}$  at 8.16 TeV with EPS09 and additional  $k_T$  broadening, (c) Pb+Pb collisions at 5 TeV with central EPS09 only, and (d)  $R_{AA}$  at 5 TeV with EPS09 and additional  $k_T$  broadening.

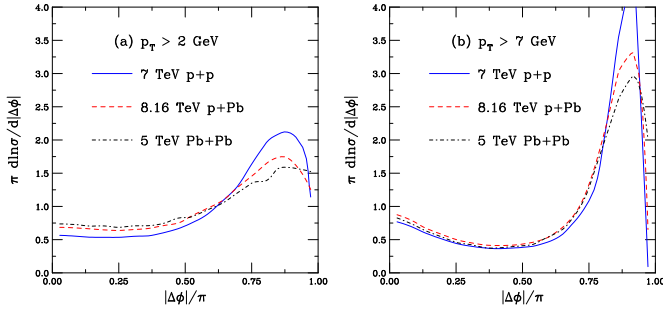


FIG. 13: (Color online) The  $b\bar{b}$  azimuthal separation for  $p_T > 2$  (a) and 7 GeV (b) for  $p+p$  collisions at 7 TeV (solid blue),  $p$ +Pb collisions at 8.16 TeV (dashed red) and Pb+Pb collisions at 5 TeV (dot-dashed black). The  $p$ +Pb calculations include shadowing and enhanced broadening ( $2\Delta$ ) while the Pb+Pb calculations include shadowing, broadening ( $4\Delta$ ), and fragmentation function modification.